JOURNAL OF MATERIALS SCIENCE 26 (1991) 263–273

Physical and mechanical properties of Si_3N_4 sintered from shock-activated and unshocked powders

S-M. CHU*, P. A. LESSING‡
New Mexico Institute of Mining and Technology, Socorro, New Mexico 87801, USA

Si_3N_4 powder was shock activated using impact from a sabot accelerated in a light gas gun. The surface area of the shocked powder increased with the square of the impact velocity. The surface energy per gram was shown to increase linearly with the kinetic energy of the sabot (including flyer plate). The shocked (green) densities of the resulting pellets were between 60 and 70% of theoretical density using calculated impact pressures between 0.16 and 1.45 GPa. The unshocked samples achieved 90 and 98% theoretical density after sintering; lower final densities in the shocked samples were attributed to microcracks which could not be completely eliminated by sintering. The values of hardness and fracture toughness were measured (after sintering) using an indentation technique. These values were higher for the shocked samples (measured in microcrack free areas) than for the unshocked samples.

1. Introduction

Sintered Si_3N_4 is used in structural and mechanical components for high temperature applications. Most "as-received" silicon nitride powders are highly agglomerated crystallites. For successful sintering, these powders must undergo traditional comminution methods: ball milling, jet milling, or attrition milling. Often these techniques are inefficient at fracturing the ceramic crystallites and are considered successful if they merely break down the agglomerates into individual crystals. In general, these traditional grinding (comminution) techniques are time consuming and expend significant energy concomitant with contamination from the jars and milling media.

The purpose of this study was to use shock waves to comminute the powders and investigate the effect on the final mechanical properties of the sintered Si_3N_4. The use of shock waves is a potential method to eliminate the disadvantages of traditional methods of grinding. Based on previous studies [1–6], a shock wave should reduce the particle size and fracture agglomerates of ceramic powders while also introducing additional point defects, residual strains and high dislocation densities within the shocked particles. By increasing the energy of the microstructure in these ways, the sinterability of shocked Si_3N_4 powder should be enhanced without significant contamination.

2. Experimental procedure

2.1. Material

Two grades of Si_3N_4 powders were supplied by Elkem Materials Company. One was ground by jet milling (designated EJ) and the other was ground by attrition milling for 7 h after jet milling (designated EA). A third Si_3N_4 powder was obtained from UBE Industries, Inc. (Type SN-E10).

The particle size distribution and chemical compositions of these "as-received" powders are shown in Tables I and II. Using X-ray diffraction, the alpha phase content in Elkem's powder was determined to be 82% while in the SN-E10 it was 95%. The BET

TABLE I Particle size distribution of "as-received" Si_3N_4 powders

	Diameter (μm)	Cumulative % retained
Elkem powder ground	10	10
by jet milling	8	10
$D_{50} = 2.50$	6	14
	4	27
	2	58
	1	75
Elkem powder ground	1	10
by attrition milling	0.8	20
$D_{50} = 0.54$	0.6	40
	0.4	64
	0.2	84
	0.1	91
Ube SN-E10 powder	1	7
$D_{50} = 0.24$	0.8	8
	0.6	12
	0.4	23
	0.2	59
	0.1	88

Present address: General Ceramics, Inc., Ceramic Systems Div., 2780 Coronado St, Anaheim, California, 92806, USA.
‡*Present address*: Idaho National Engineering Laboratory, Materials Technology, PO Box 1625, Idaho Falls, Idaho 83415, USA.

0022–2461/91 $03.00 + .12

TABLE II Chemical analysis of "as-received" Si_3N_4 powders

	Composition (wt %)								
	Al	C	Ca	Fe	O	"Free" Si	Y	Cl	N
Elkem powder ground by jet milling	< 0.07	0.9	< 0.01	0.004	1.7	1.1	—	—	—
Elkem powder ground by attrition milling	0.31	1.62	0.015	0.03	4.2	—	0.49	—	—
Ube SN-E10 powder	< 50 p.p.m.	< 0.2	< 50 p.p.m.	< 100 p.p.m.	< 2.0	—	—	< 100 p.p.m	> 38.0

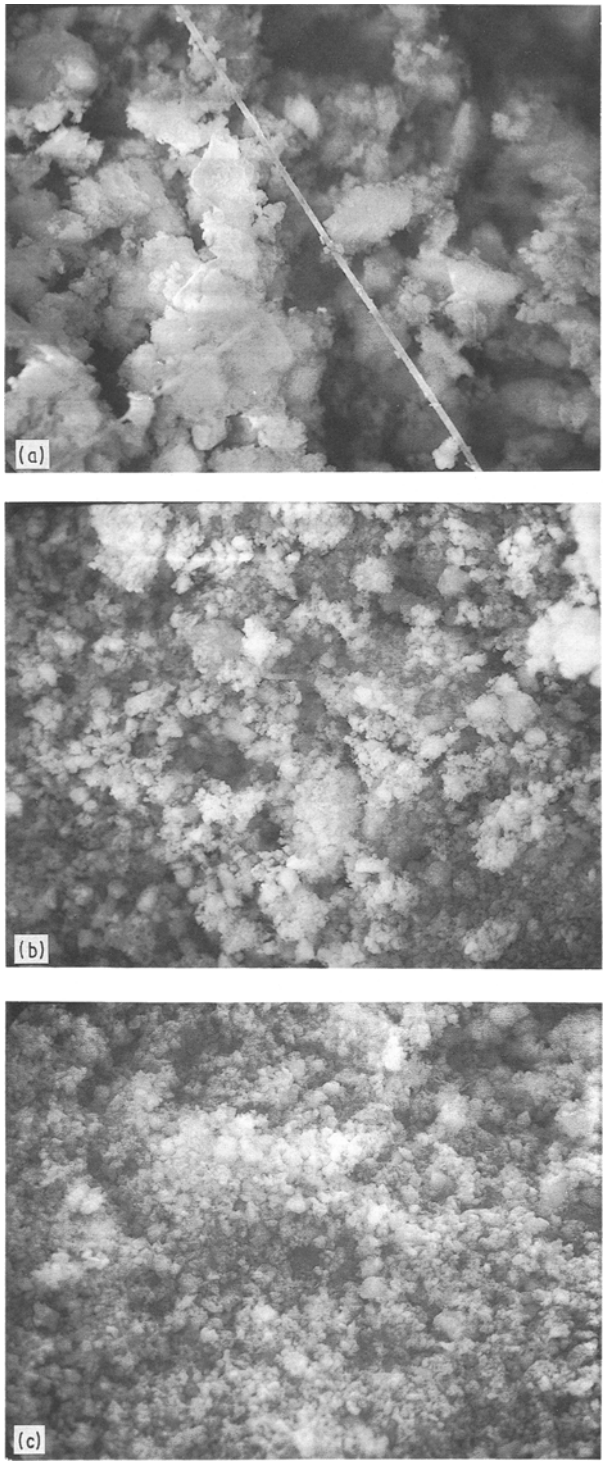

Figure 1 SEM micrographs of "as-received" Si_3N_4 powders. (a) Elkem powder ground by jet milling (× 3500), (b) Elkem powder ground by attrition milling (× 3500), (c) Ube SN-E10 powder (× 3500).

specific surface areas were: (1) EJ: 6.38 $m^2 g^{-1}$, (2) EA: 14.5 $m^2 g^{-1}$, and (3) UBE SN-E10: 10.8 $m^2 g^{-1}$.

Fig. 1 shows SEM micrographs of the powder in the as-received form. The as-received powder supplied by Elkem was very "fluffy" and was composed of porous aggregates of submicrometre crystallites with some large aspect-ratio whiskers. The aspect ratio of whiskers in the attrition-milled powder was smaller than in the jet-milled powder. In Ube's SN-E10 powder there were no big agglomerates or whiskers, and its particles were smaller than those found in Elkem's powders.

Sintering aids used in the study were yttria and alumina. The yttria was supplied by Union Molycorp, Inc. (grade 5600) and the alumina was from Baikalox (grade CR30).

2.2. Specimen preparation and test methods

Powder processing prior to shocking is shown in Fig. 2. A light gas gun was used to conduct the fracture experiments. Compressed helium gas was used to accelerate the projectile (sabot plus flyer plate). Two laser beams located at the end of the barrel were used to evaluate the velocity of the projectile. Before firing the gas gun, the gun barrel was evacuated three times to a pressure of 500 mtorr in order to avoid driving a strong shock wave of air ahead of the projectile.

Two groups of EJ Si_3N_4 material were used for the shock test. One utilized no sintering aids and had a loading density of 1.05 $g cm^{-3}$. The other used sintering aids and had a loading density of 1.30 $g cm^{-3}$. Samples with no sintering aids were reground, in a hand mortar, after the shock test and were evaluated using BET specific surface area, particle size distribution measurement and X-ray diffraction analysis. The unshocked samples were dry pressed under 69 000 kPa (10 000 psi) in a 13 mm internal diameter steel die. The thickness of all the samples was about 3.75 mm and they typically weighed approximately 0.8 g.

After the powders were either exposed to the shock wave (dynamic compaction) or dry-pressed, the samples were sintered. The conditions of the pressureless sintering are shown in Fig. 3. All the samples were packed with a protective powder and held in a graphite crucible. After sintering, their bulk density was determined by using a liquid displacement method. A linear pore-counting technique [7] was used to measure porosity which then was used to

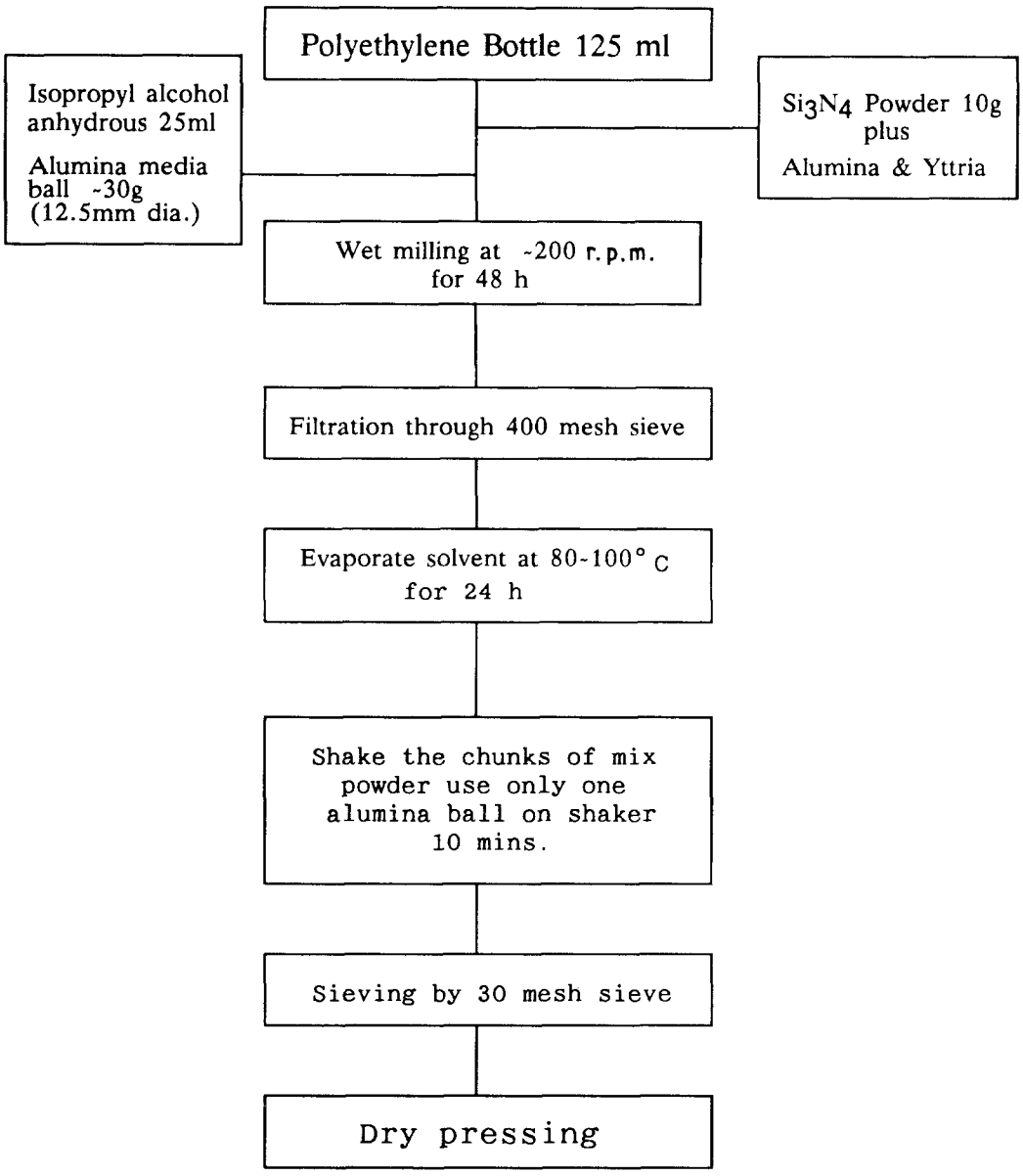

Figure 2 Powder processing prior to dynamic comminution (shocking).

calculate the theoretical density of sintered samples. The model of Yeheskel and Gefens [8] was used to calculate the Young's modulus of each sintered sample. An indentation technique [9, 10] was used to determine the hardness and toughness of the sintered samples.

A glass phase exists in the grain boundaries of sintered Si_3N_4 that affects its mechanical properties. It was important to determine the volume of the glass phase since the volume varied with the oxygen content of the Si_3N_4 and the amount of oxide sintering aids that were added. There were two assumptions made prior to performing the theoretical density and volume of glass phase calculation. First, no nitrogen exists in the glass phase. Second, the atom sizes in the glass are the same and the structures have the same atomic packing factor (APF). Using these assumptions, and one measurement for the bulk density of $Y_{0.166}\,Si_{0.15}\,Al_{0.032}\,O_{0.651}$ to be $3.83\,g\,cm^{-3}$ (as given by Loehman [11]), the densities for all the glass phases were calculated. From the weight and density of glass and Si_3N_4, the volume per cent for these two phases were then calculated. The results of these calculations are shown in Table III.

3. Results

3.1. Physical properties of the shocked samples

There was an increase in green compact density with shock pressure. The density increased very fast at pressures under 0.3 GPa. The compact's densities were in a very useful range (from about 60 to 77% of theoretical density). The densities were much better than usually gained from dry isostatic pressing at high pressures and had good strength, yet the compact was not too hard to be amenable to green machining.

The results of the specific surface area tests are plotted in Fig. 4. The measured surface area of the powder increased from 6.38 to about $15.3\,m^2\,g^{-1}$. This result indicates that individual crystallites were being fractured by the process. There was a power law increase in surface area with increased projectile velocity. By discrete least-squares approximation [12], the

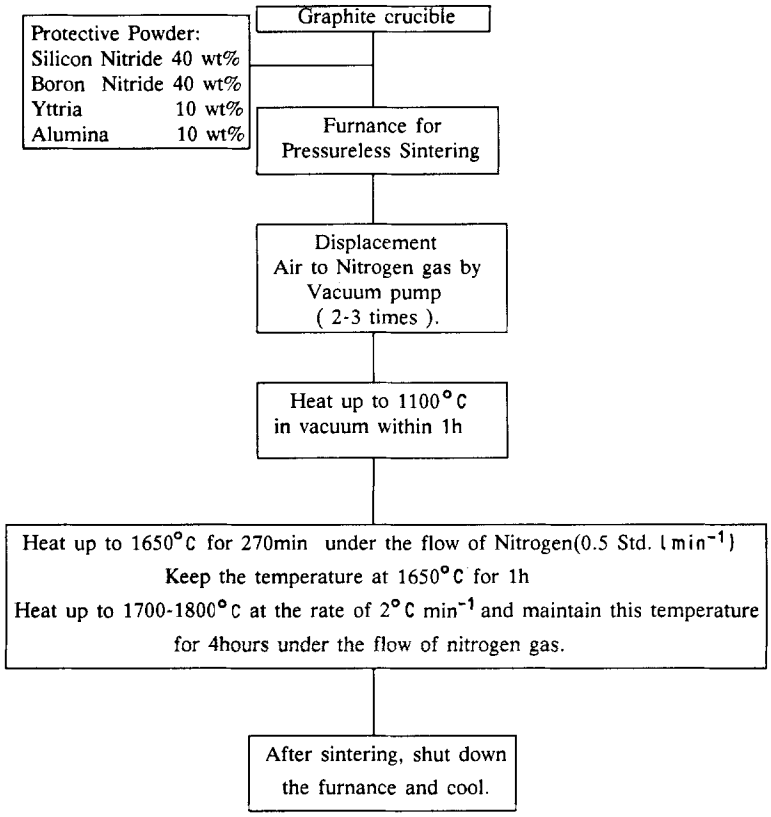

Figure 3 Procedure and conditions for pressureless sintering.

TABLE III Results of theoretical calculation of volume of liquid phase present during sintering of various Si_3N_4 powders with sintering aids

Materials	Al_2O_3 (g)	Y_2O_3 (g)	SiO_2 (g)	Si_3N_4 (g)	Volume of liquid (cm^3)	Volume of solid (cm^3)	Vol % of liquid
EJ	5.5	5.0	2.85	86.7	4.12	27.2	13.2
EJ	2.5	2.5	3.03	92.0	2.60	28.8	8.27
EJ	7.5	7.5	2.71	82.3	5.29	25.8	17.0
EJ	2.0	6.0	2.93	89.1	2.98	27.9	9.64
EA	5.5	5.0	5.44	84.1	5.14	26.4	16.3
EA	2.5	2.5	5.78	89.2	3.68	28.0	11.6
EA	7.5	7.5	5.17	79.8	6.24	25.0	20.0
EA	2.0	6.0	5.59	86.4	4.03	27.1	13.0
Ube	5.5	5.0	3.36	86.1	4.33	27.0	13.8
Ube	2.5	2.5	3.56	91.4	2.81	28.7	8.92
Ube	7.5	7.5	3.19	81.8	5.48	25.6	17.6
Ube	2.0	6.0	3.45	88.6	3.18	27.8	10.3

curve in Fig. 4 can be expressed as

$$A = A_0 + 7.63 \times 10^{-3} V_F^2 \quad (1)$$

where A is post-shock surface area in $m^2 g^{-1}$, A_0 the initial surface area, and V_F the projectile velocity. This result is logical since the energy input into the powder is proportional to the velocity squared of the projectile.

If we consider a fraction of the kinetic energy of the projectile is converted into new surface area, Equation 1 can be rewritten as

$$\gamma \Delta A_t = \beta \tfrac{1}{2} m V_F^2$$

where γ is the surface energy of Si_3N_4, ΔA_t is the total new surface area created by the shock treatment, $\frac{1}{2}mV_F^2$ the kinetic energy of the projectile, and β the fraction of kinetic energy of the projectile converted to new surface area. The fraction factor was calculated to be about 0.032. This result is shown in Fig. 5. The new surface energy per sample increased linearly with the kinetic energy of the projectile.

Fig. 6 compares the particle size distribution of the "as-received" powders to that of the shocked powder. The "particle size" measured by the sedimentation technique includes both discrete particles and agglomerates. The D_{50} of the as-received EJ powder is 2.5 μm. The D_{50} of the shocked powder (336 m sec^{-1}) is 2.3 μm, but the amount of powder in the size range below 0.5 μm is more than the as-received EJ powder.

Fig. 7 shows SEM photos of shocked-compacted

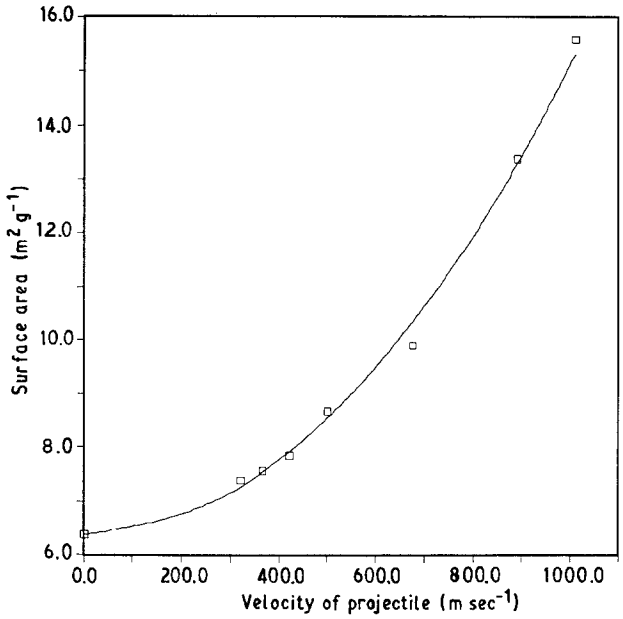

Figure 4 Specific surface area (BET) for powders compacted in gas gun as a function of impact velocity.

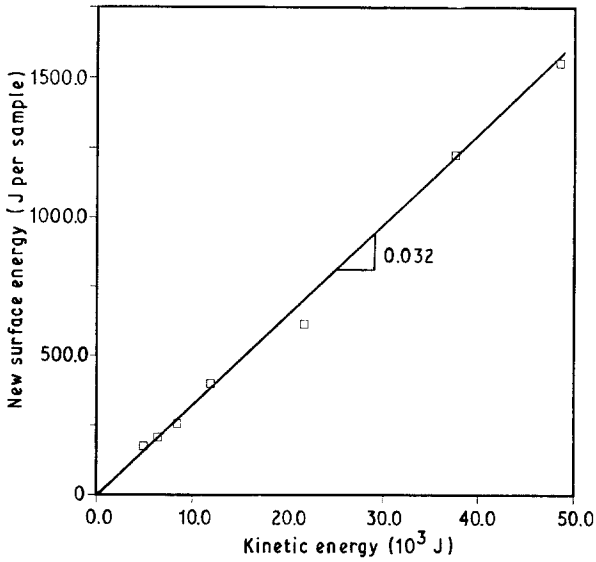

Figure 5 Additional surface energy (J per sample) created in sample during dynamic comminution as a function of projectile kinetic energy.

surfaces. When compared to "as-received" powders (see Fig. 1), the surface shows powder with crystallites that are easier to distinguish and are possibly smaller than the "as-received EJ" jet-milled Elkem powder. Powder no. 2 was shocked at $v = 421\ \mathrm{m\,s^{-1}}$ while powder no. 3 was shocked at $v = 366\ \mathrm{m\,s^{-1}}$. Powder no. 2 (the more heavily shocked sample) appears to have a smaller average crystallite size than powder no. 3.

The Sedigraph and SEM evidence combine to indicate that the strong bonding between the crystals in the agglomerate have been broken. The SEM also shows that all of the whiskers have disappeared in the shocked powder.

The shocked powders show a strong resemblance in morphology to both the Ube SN-E10 and attrition-milled Elkem powder. Regrinding the shocked compact (using a mortar and pestle) does not break up the compact entirely into individual crystallites.

X-ray diffraction analysis showed there were no new compounds created in the shocked samples. A line broadening analysis was conducted using a computerized Warren–Averbach method [15]. The integral line breadth increased with shock velocity. By

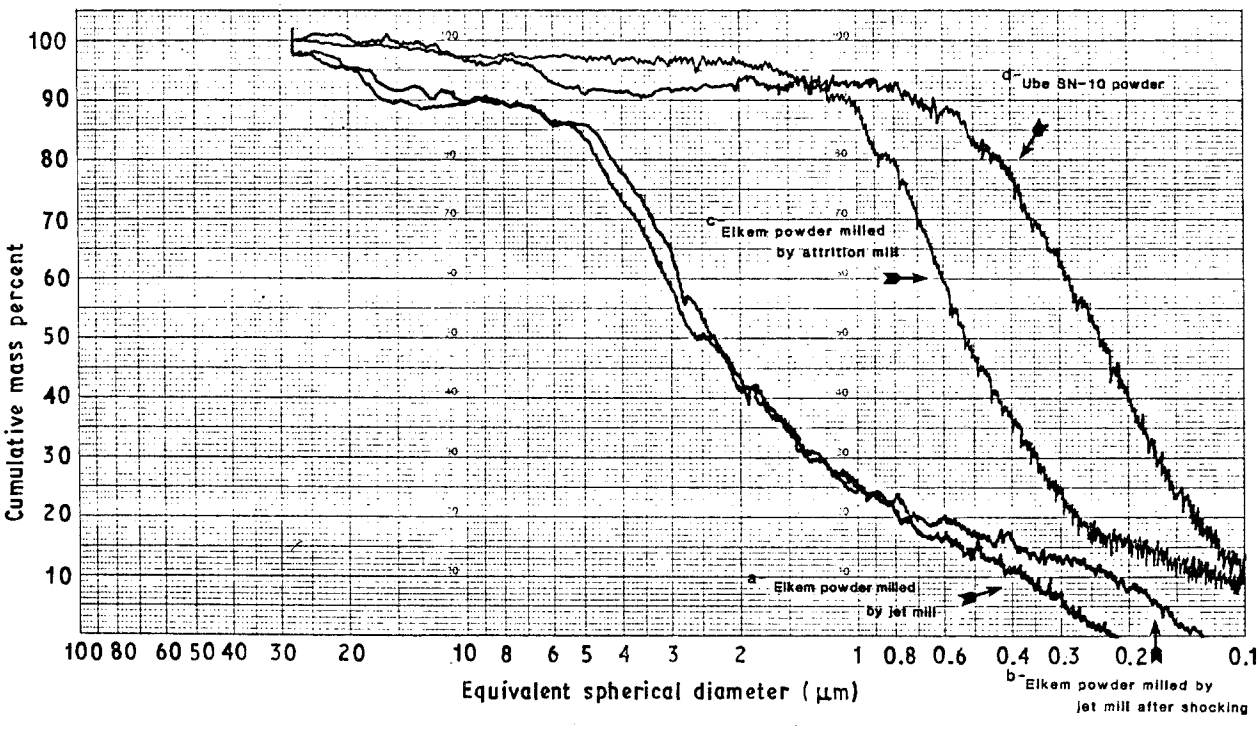

Figure 6 Particle size distribution as measured by "Sedigraph" for Elkem Si_3N_4 comminuted by jet milling, attrition milling, and dynamic shocking. (Ube for comparison).

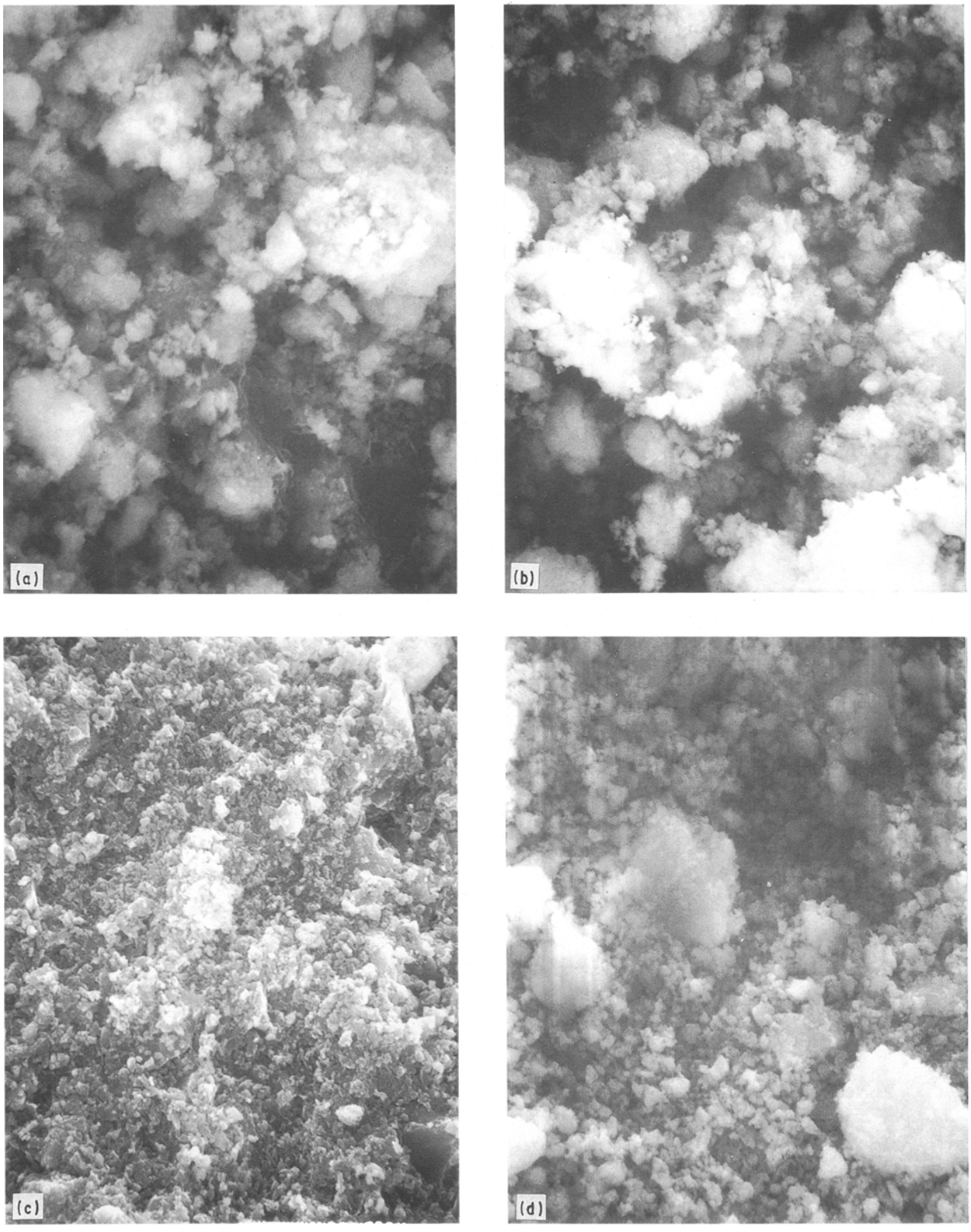

Figure 7 SEM micrographs of shock comminuted powder pellets. (a) Powder No. 2 reground by hand (× 3500), (b) Powder No. 3 reground by hand (× 3500), (c) Fracture surface of shocked powder No. 2 (× 3500), (d) Fracture surface of shocked powder No. 3 (× 3500).

comparing the heavily shocked ($v = 1010\,\mathrm{m\,s^{-1}}$) sample with a lightly shocked ($v = 321\,\mathrm{m\,s^{-1}}$) sample, the crystallite size decreased and microstrain increased.

3.2. Properties of post-sintered samples

After sintering, X-ray diffraction showed there was no α-Si_3N_4 remaining. The theoretical density (TD) of the different compositions (as determined by the pore-counting technique) were as follows

Si_3N_4 + Y6.0%, A2.0% TD = $3.279\,\mathrm{g\,cm^{-3}}$

Si_3N_4 + Y2.5%, A2.5% TD = $3.232\,\mathrm{g\,cm^{-3}}$

Si_3N_4 + Y5.0%, A5.5% TD = $3.275\,\mathrm{g\,cm^{-3}}$

Si_3N_4 + Y7.5%, A7.5% TD = $3.279\,\mathrm{g\,cm^{-3}}$

TABLE IV Calculated percentage of theoretical density from immersion measurements of pellets sintered from unshocked powders

Materials	Temperature (°C)				
	1700	1725	1750	1780	1800
EA Y6.0% A2.2%	98.77	99.50	99.44	99.47	99.56
EJ Y6.0% A2.0%	96.30	98.53	98.83	98.95	99.17
Ube Y6.0% A2.0%	89.96	95.87	97.95	98.43	98.71
EA Y2.5% A2.5%	96.49	99.06	99.00	99.59	99.03
EJ Y2.5% A2.5%	75.52	87.46	89.35	95.60	89.53
Ube Y2.5% A2.5%	91.58	96.74	98.54	99.00	98.75
EA Y5.0% A5.5%	98.23	98.81	98.72	98.78	98.66
EJ Y5.0% A5.5%	97.98	98.32	98.44	98.56	98.32
Ube Y5.0% A5.5%	98.47	98.72	98.69	98.81	98.69
EA Y7.5% A7.5%	99.66	99.75	99.75	99.87	99.66
EJ Y7.5% A7.5%	98.22	98.95	98.71	99.32	99.05
Ube Y7.5% A7.5%	99.54	99.47	99.50	99.63	99.50

Estimated precision ± 0.03.

TABLE VI Vickers hardness values (GPa) measured on samples sintered from unshocked powders

Materials	Temperature (°C)				
	1700	1725	1750	1780	1800
EA Y6.0% A2.0%	15.9	15.3	15.2	16.0	15.7
EJ Y6.0% A2.0%	16.1	15.8	15.9	15.8	16.1
Ube Y6.0% A2.0%	17.8	17.0	16.8	17.7	16.7
EA Y2.5% A2.5%	16.5	16.2	15.5	16.4	16.0
EJ Y2.5% A2.5%	bad	15.6	15.6	16.0	16.1
Ube Y2.5% A2.5%	17.5	17.6	17.0	17.7	17.4
EA Y5.0% A5.5%	15.4	16.3	15.3	15.8	15.6
EJ Y5.0% A5.5%	15.8	16.1	15.9	16.0	15.7
Ube Y5.0% A5.5%	17.5	18.7	16.7	16.2	16.6
EA Y7.5% A7.5%	14.9	15.1	15.0	15.0	15.2
EJ Y7.5% A7.5%	15.4	15.4	15.1	15.2	15.2
Ube Y7.5% A7.5%	16.2	17.0	16.7	16.5	16.6

Estimated precision ± 0.04.

where Y corresponds to yttria and A is alumina. Using the TD value, the percentage of TD for every sample can be calculated. Table IV shows the percentage of TD for different unshocked samples sintered at a variety of temperatures. For most cases, 1780 °C seems to be the "best" sintering temperature.

Table V shows the sintered densities produced from shocked samples. Within this group, the trend of all the compositions is for higher shock pressures to produce higher density samples, however, comparison with Table IV shows that unshocked samples have slightly higher densities after sintering than shock-activated samples.

Table VI shows the hardness values measured for all the unshocked samples which were sintered at different temperatures. Generally, the hardness increased with increased sample density, a small grain size, or a decreased volume of glass phase.

The value of Vicker's hardness measured on shock activated and sintered Si_3N_4 samples is shown in Table VII. The testing area was chosen in areas free of microcracks as observed at 400 × under an optical microscope. In general, the value of hardness was in the range of 15 to 16.5 GPa. EJ A2.5%, Y2.5% shocked using $v = 871\ m\,s^{-1}$ and sintered at 1700 °C gave, however, Vicker's hardness values up to 17.3 GPa. When comparing the values of Table VII with those of Table VI, the hardness values of samples from shocked powders are higher than the hardness values of the unshocked samples. This is especially true for samples shocked using $v = 550$ to $650\ m\,s^{-1}$.

Using Table VIII one can compare the toughness of various unshocked materials which have the same amount of sintering aids. The compositions that have smaller values of toughness are the same ones which have a larger starting particle size. The toughness values "bounce around" with increases in the volume of glass phase, but there is a tendency for the toughness to increase slightly when increasing the percent of liquid (glass) when going from the Y2.5% + A2.5%

TABLE V Calculated percentage of theoretical density from immersion measurements of pellets sintered from shocked powder pellets

Materials	Shock velocity ($m\,sec^{-1}$)	1700 °C		1750 °C		1775 °C	
		Shocked density % TD	Sintered density % TD	Shocked density % TD	Sintered density % TD	Shocked density % TD	Sintered density % TD
EJ A2.0% Y6.0%	380	62.9	76.0	64.6	81.6	63.3	81.6
EJ A2.0% Y6.0%	625	70.8	97.0	71.1	96.4	70.6	96.8
EJ A2.5% Y2.5%	382	62.1	86.4	62.6	90.4	61.7	90.4
EJ A2.5% Y2.5%	580	69.2	94.4	69.5	96.1	68.7	96.2
EJ A2.5% Y2.5%	871	76.6	97.8	75.2	94.5	74.2	93.5
EJ A5.5% Y5.5%	383	63.0	97.1	63.9	97.0	63.0	96.7
EJ A5.5% Y5.5%	560	68.5	97.5	69.9	95.9	68.9	97.3
EJ A7.5% Y7.5%	398	65.8	97.9	65.2	97.9	64.5	98.1
EJ A7.5% Y7.5%	424	65.8	98.4	66.2	97.9	64.9	97.9
EJ A7.5% Y7.5%	621	71.2	97.4	70.8	97.2	70.0	96.6

Estimated precision ± 0.05.

TABLE VII Vickers hardness values measured on samples sintered from shock compacted pellets. (Measured in areas with no visible microcracks)

Materials	Shock velocity ($m\,sec^{-1}$)	Temperature (°C)		
		1700	1755	1775
EJ A2.0% Y6.0%	380	Bad	Bad	Bad
EJ A2.0% Y6.0%	625	16.0	15.7	16.6
EJ A2.5% Y2.5%	382	Bad	12.6	13.7
EJ A2.5% Y2.5%	580	15.6	15.2	16.0
EJ A2.5% Y2.5%	871	17.3	15.8	16.3
EJ A5.5% Y5.0%	383	16.2	15.9	15.7
EJ A5.5% Y5.0%	560	16.2	16.2	16.4
EJ A7.5% Y7.5%	398	15.0	15.2	15.2
EJ A7.5% Y7.5%	424	15.4	15.2	15.4
EJ A7.5% Y7.5%	621	15.5	15.4	15.4

Estimated precision ± 0.03.

TABLE VIII Toughness ($MN\,m^{-3/2}$) measured by indention technique of samples sintered from unshocked powders

Materials	Temperature (°C)				
	1700	1725	1750	1780	1800
EA Y6.0% A2.0%	3.90	3.89	3.81	3.27	4.54
EJ Y6.0% A2.0%	3.32	3.41	3.77	2.94	3.54
Ube Y6.0% A2.0%	3.80	4.53	4.37	3.98	4.04
EA Y2.5% A2.5%	3.45	3.68	3.42	3.87	3.58
EJ Y2.5% A2.5%	bad	2.95	2.99	3.37	2.87
Ube Y2.5% A2.5%	3.19	3.87	3.77	3.75	4.03
EA Y5.0% A5.5%	3.72	4.13	3.62	3.74	3.94
EJ Y5.0% A5.5%	3.20	3.84	3.57	2.95	2.59
Ube Y5.0% A5.5%	3.85	4.20	4.39	4.19	4.16
EA Y7.5% A7.5%	3.95	3.92	3.88	3.46	3.86
EJ Y7.5% A7.5%	3.33	3.61	3.21	2.20	2.42
Ube Y7.5% A7.5%	4.40	4.06	4.33	3.50	2.82

Estimated precision ± 0.05.

TABLE IX Toughness ($MN\,m^{-3/2}$) measured by indention technique of samples sintered from shocked pellets. (Measurement in areas with no visible micro-cracks)

Materials	Shock velocity ($m\,sec^{-1}$)	Temperature (°C)		
		1700	1755	1775
EJ A2.0% Y6.0%	380	Bad	Bad	Bad
EJ A2.0% Y6.0%	625	3.35	3.05	3.70
EJ A2.5% Y2.5%	382	Bad	3.78	3.16
EJ A2.5% Y2.5%	580	3.43	3.57	3.60
EJ A2.5% Y2.5%	871	3.16	3.02	3.24
EJ A5.5% Y5.0%	383	3.29	3.37	3.40
EJ A5.5% Y5.0%	560	3.27	3.50	3.45
EJ A7.5% Y7.5%	398	2.59	3.30	3.22
EJ A7.5% Y7.5%	424	2.83	3.25	3.14
EJ A7.5% Y7.5%	621	2.52	3.00	3.43

Estimated precision ± 0.05.

additives to the Y6.0% + A2.0% and then to decrease at the highest additive level (Y7.5% + A7.5%) where the glass volume approaches 17 to 20 vol%. The shock activated and sintered samples showed improved toughness when sintered at 1750 to 1775 °C. The toughness data of shocked samples is shown in Table IX.

Fig. 8 shows the fracture surface of unshocked Si_3N_4 + Y6.0% + A2.0% materials sintered at 1800 °C. The EJ material's fracture surface is more smooth and has more transgranular structure than the fracture surfaces of samples made from EA or Ube material. Very few rod-shaped grains can be found in EJ material but many more rod-shaped grains can be found in the EA material.

4. Discussion

A comparison of the specific surface area and the particle size distribution results (after shock treatment) with the SEM data would indicate that the surface area is a more reliable indicator of the actual fracture of crystallites. The particle size analysis, using sedimentation, is dependent on proper deagglomeration and deflocculation of the crystallites during the measurement procedure. Also, the sedimentation technique only measures the weight fraction of powders. Therefore, it takes a very large number of small particles to add up to a small change in weight distribution.

Higher shock pressure causes more microcracks in the specimens. Some of these cracks are fairly small and isolated. They become rounded during sintering as shown in Fig. 9. Larger cracks can be found in specimens impacted at higher shock pressures as shown in Fig. 10. These cracks become wider and longer during the sintering process. Both cracks contribute to a lowered sintered density; as measured by the liquid displacement technique.

The weight loss data, after sintering, showed shocked samples had more weight loss and the values increased with shock velocity. This may be because these samples had more microcracks which correspond to a large surface area exposed to the gas atmosphere. The increased area can lead to more glass phase evaporation and Si_3N_4 decomposition.

The hardness of the glass grain-boundary phase is much lower than the Si_3N_4 [13]. Since all the hardness indentations were made in areas without cracks, and if the densities of the samples are very close to the same value then samples having less glass phase and smaller grain sizes should show enhanced hardness. This is shown by a careful comparison of Table III, Table VI, and Fig. 8. When sintered to the same temperature, EJ material had the largest grain size, EA material showed slightly smaller grains, and Ube had a significantly smaller grain size.

Two further trends can be observed for the shocked and sintered materials in Table VII: (1) the hardness increased with shock pressure, and (2) the hardness initially increases with the amount of glass phase and then drops at the highest level.

In general, the toughness value is influenced by

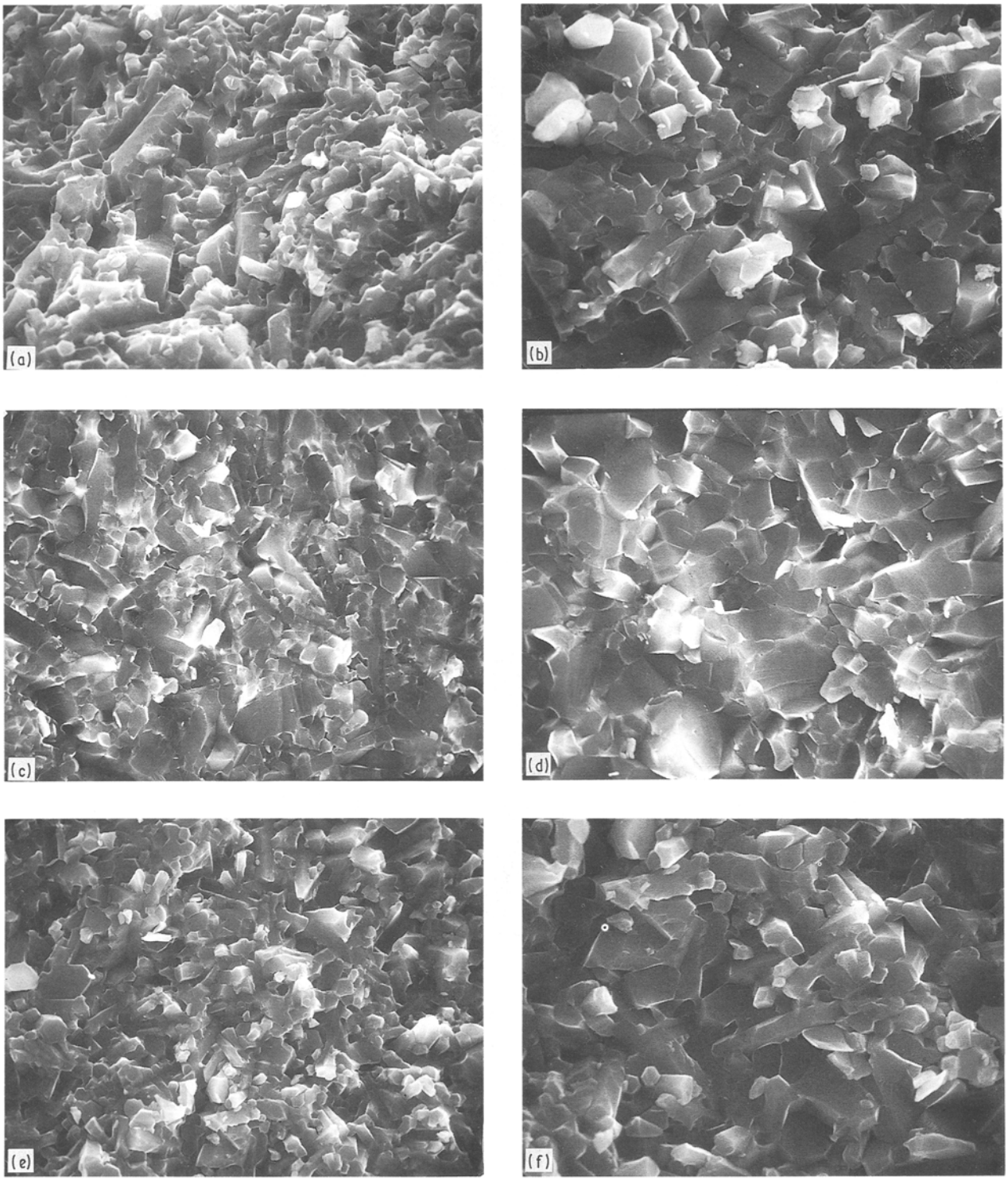

Figure 8 SEM micrographs of fracture surfaces of samples sintered from unshocked powders at 1800 °C (all have same nominal composition) (a) EA Y6.0% A2.0% (× 5000), (b) EA Y6.0% A2.0% (× 10000), (c) EJ Y6.0% A2.0% (× 5000), (d) EJ Y6.0% A2.0% (× 10000), (e) Ube Y6.0% A2.0% (× 5000), (f) Ube Y6.0% A2.0% (× 10000).

grain size, grain shape, porosity, and amount and type of glass phase. In Table VIII, the materials which have smaller values of toughness are the same materials which have bigger starting particle sizes. The increase with toughness with increased glass phase (at the smaller additive levels) is an indication of better bonding and higher densities. The density increase can be seen by examination of Table IV. At the highest additive levels, the large volume of glass phase begins to be detrimental to the toughness.

It is commonly accepted [14] that toughness can be enhanced by crack deflection. The deflection results in a toughening because of a reduced driving force on the deflected portion of the crack. In particular, the twisting of a crack between rod-shaped deflecting grains provides an appreciable reduction in driving force. The resultant toughening, for randomly oriented grains, depends only on the volume concentration and shape of the deflecting grains. Generally, high aspect ratio rods induce the highest toughening by virtue of

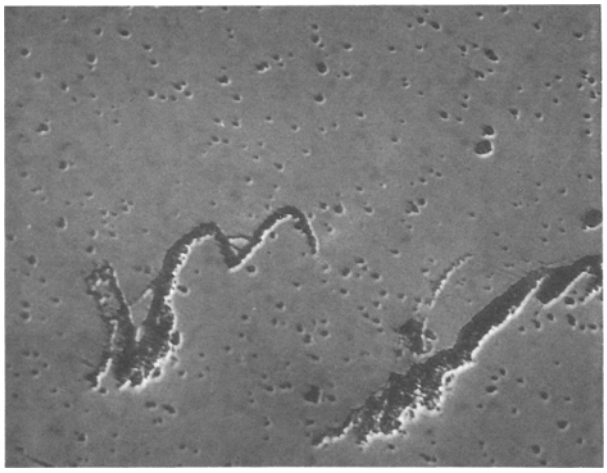

Figure 9 Optical micrograph of typical microcracks found in a sample sintered at 1750 °C from shock compacted (383 m sec^{-1}) powder. (140 ×).

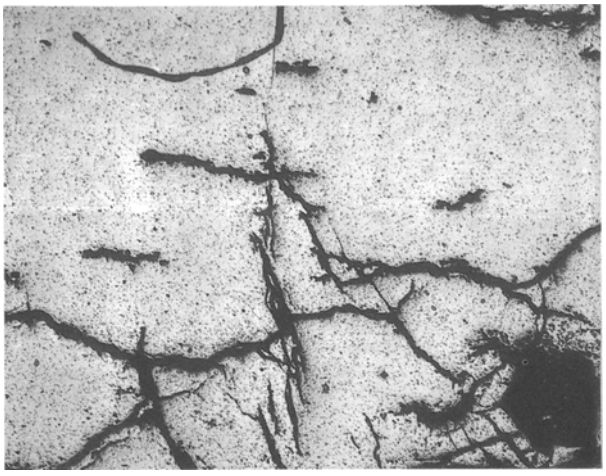

Figure 10 Optical micrograph of cracked area of sample sintered at 1750 °C from shock compacted (871 m sec^{-1}) powder. (14 ×).

their influence on the high twist angles and the toughness values are independent of grain size. The microstructures of Fig. 8 and the fracture toughness data in Table VIII show agreement. The EJ material has more transgranular fracture and this corresponds to a lower value of fracture toughness.

5. Conclusions

It was demonstrated that Si_3N_4 ceramic powders can be shock comminuted. In samples sintered after shocking, the hardness and fracture toughness of shocked samples were better than unshocked samples of the same starting materials. Cracking in pellets impacted at high velocities would undoubtedly lead to severely reduced strength values in sintered samples. Breaking up the compacted pellets and re-pressing of the powders comminuted at the high velocities would then be necessary before sintering.

Additional conclusions are as follows.

(1) The compact's green density, surface area, and amount of very fine particles were enhanced by shock exposure. The density increased very fast at pressures less than 0.3 GPa.

All the whiskers in as-received Elkem powders were broken after shock treatment and the density of the shocked samples was greater than 60% of theoretical density. The crystallite sizes observed on the fracture surface of the compacts were much smaller than the starting powder. Quantitative X-ray analysis indicated the decrease in crystallite size was real and it was accompanied by an increase in microstrain.

The surface area data showed the surface area of the particles increased with velocity and followed a power law. The conversion of kinetic energy to surface energy was found to be 0.032.

(2) The best sintering temperature was found to be between 1780 and 1800 °C. The sintered densities were as high as 99% TD, with no alpha phase detected. Based on the indentation technique, Vicker's hardness values were between 15 and 18 GPa. Ube's material had the highest Vicker's hardness values regardless of the amount of sintering additives. This was attributed to the finer starting particle size of its powder, which resulted in a finer grain size in the sintered sample or perhaps a decreased volume of glass phase.

Fracture toughness values were between 3.5 and 4.5 MN m$^{-3/2}$ (using an indentation technique). These values were typically smaller than those evaluated by other toughness measurement techniques. The materials which showed smaller toughness values were those which had bigger starting particle size and less volume of glass phase. The fracture surfaces which showed high aspect ratio rod-shaped grains correlated to enhanced toughness.

(3) Samples which had high green densities (from shocking) did not obtain higher sintered densities. This was attributed to the higher shock pressure which induced more microcracks in the specimens. Hardness measured in uncracked regions of samples shocked using $v = 500$ to 650 m sec^{-1} had higher values than the unshocked samples.

In general, the toughness for samples sintered from shocked pellets were between 3.00 and 3.80 MN m$^{-3/2}$ which was better than those measured on samples sintered from unshocked pellets.

References

1. M. A. MEYERS and L. E. MURR, in "Shock Waves and High-Strain-Rate Phenomena in Metals", edited by M. A. Meyers and L. E. Murr (Plenum, New York, 1981) p. 487.
2. O. R. BERGMANN and J. BARRINGTON, *J. Amer. Ceram. Soc.* **49** (1966) 502.
3. J. J. PETROVIC, B. W. OLINGER and R. B. ROOF, *J. Mater. Sci.* **20** (1985) 391.
4. Y. K. LEE and F. L. WILLIAMS, *J. Mater. Sci.* **20** (1985) 2488.
5. E. K. BEAUCHAMP, R. E. LOEHMAN, R. A. GRAHAM, B. MOROSIN and E. L. VENTURINI, in "Emergent Process Methods for High-Technology Ceramics", edited by R. F. Davis, H. Palmour III and R. L. Porter (Plenum, New York, 1984) p. 735.
6. T. AKASHI and A. B. SAWAOKA, in "High Pressure Explosive Processing of Ceramics", edited by R. A. Graham and A. B. Sawaoka (Trans Tech Publications, Switzerland, 1987) p. 87.

7. A. L. RUOFF, "Materials Science" (Prentice-Hall, Englewood Cliffs, NJ, 1973) p. 336.
8. O. YEHESKEL and Y. GEFENS, *Mater. Sci. Engng.* **71** (1985) 95.
9. G . R. ANSTIS, P. CHANTIKUL, B. R. LAWN and D. B. MARSHALL, *J. Amer. Ceram. Soc.* **64** (1981) 533.
10. A. G. EVANS and E. A. CHARLES, *ibid.* **59** (1976) 371.
11. R. E. LOEHMAN, *ibid.* **62** (1979) 491.
12. R. L. BURDEN and J. D. FAIRES, "Numerical Analysis", 3rd edn (PWS Publisher, Boston, MA, 1985) p. 360.
13. O. YEHESKEL and Y. GEFEN, *Mater. Sci. Engng.* **78** (1986) 209.
14. A. G. EVANS, "Fracture in Ceramic Materials" (Noyes Publications, Park Ridge, NJ, 1984) p. 32.
15. B. E. WARREN, "Progress in Metal Physics", Vol. 8 (Pergamon, London, 1959) p. 147.

Received 5 September 1989
and accepted 19 February 1990